

# Detection of Proteins in Serum by Micromagnetic Aptamer PCR (MAP) Technology\*\*

Andrew Csordas, Aren E. Gerdon, Jonathan D. Adams, Jiangrong Qian, Seung Soo Oh, Yi Xiao,\* and H. Tom Soh\*

The effective diagnosis and prognosis of many diseases depends on the ability to quantitatively measure protein biomarkers from clinical samples at low concentrations.<sup>[1]</sup> For example, fluctuations in serum concentrations of cytokines, such as platelet-derived growth factor-BB (PDGF-BB), can serve as indicators of tumor angiogenesis,<sup>[2]</sup> whereas levels of virus-related proteins such as hemagglutinin can indicate progression of an infection.<sup>[3]</sup> Accurate detection of diagnostic biomarkers in blood is often challenging because of its complex composition comprising thousands of proteins with concentrations ranging over 12 orders of magnitude.<sup>[4,5]</sup> Albumin, for example, constitutes approximately half of the total serum protein (30–50 mg mL<sup>-1</sup>), while many important disease-related biomarkers exist at concentrations as low as 1 pg mL<sup>-1</sup>.<sup>[4,5]</sup>

Enzyme-linked immunosorbent assay (ELISA) is a standard approach to detect protein biomarkers directly from blood. Unfortunately, this assay can suffer from a lengthy development period for specific antibodies,<sup>[6]</sup> insufficient sensitivity,<sup>[7]</sup> limited dynamic range,<sup>[6,8,9]</sup> and long assay

times involving multiple washing steps,<sup>[10]</sup> thereby limiting its usefulness and making it impractical to implement at the point of care. Several groups have developed innovative approaches to improve the sensitivity and dynamic range of ELISAs by combining antibody-based molecular recognition with nucleic acid amplification-based detection, such as proximity ligation,<sup>[11]</sup> immuno-PCR,<sup>[12–14]</sup> and bio-barcode detection.<sup>[15]</sup> However, because interferents in blood can inhibit many amplification reactions,<sup>[16–19]</sup> there is a critical need for universal sample preparation systems that allow amplification-based detection of protein biomarkers from complex samples in a monolithic, disposable, and automated format.

Herein, we report the micromagnetic aptamer PCR (MAP) detection system, which integrates high-gradient magnetic field sample preparation in a microfluidic device with aptamer-based real-time PCR readout, to achieve highly sensitive and quantitative detection of protein targets directly from complex samples. As a model, we demonstrate the capability to quantitatively detect the cancer biomarker PDGF-BB over a wide dynamic range (62 fm to 1 nm) in a complex background of serum with clearly discernable and reproducible PCR amplification signals.

The detection assay starts with the incubation of a serum sample containing PDGF-BB target protein with magnetic beads coated with capture antibody and anti-PDGF PCR aptamers, which incorporate flanking PCR primer sequences (Figure 1A). As with ELISA,<sup>[20]</sup> the use of dual-affinity reagents significantly increases the specificity of detection. After the incubation step, the sample was loaded into a micromagnetic separation (MMS) chip, in which magnetically labeled antibody–target–aptamer complexes were trapped by the high local magnetic field gradients generated by micro-fabricated ferromagnetic structures (MFSs) patterned within the microchannel.<sup>[21,22]</sup> Meanwhile, nontarget serum proteins, unused reagents, and PCR contaminants were continuously washed out during separation (Figure 1B). After washing the trapped beads, the external magnetic field was removed, which demagnetized the MFSs thereby allowing magnetic target complexes to be eluted with phosphate-buffered saline containing 0.25 mM MgCl<sub>2</sub> (PBSM; Figure 1C). The entire separation and purification process (trapping, washing, and bead release) required about 30 min. One microliter of collected eluent was directly subjected to real-time PCR analysis, which yielded a signal proportional to the concentration of target protein in the serum sample (Figure 1D). Note that real-time PCR calibration curves with and without magnetic beads verified that the presence of  $1 \times 10^4$  antibody-coated magnetic beads per PCR reaction volume did not

[\*] S. S. Oh, Dr. Y. Xiao, Prof. H. T. Soh  
Materials Department, Department of Mechanical Engineering  
University of California, Santa Barbara  
Santa Barbara, CA 93106 (USA)  
E-mail: yixiao@physics.ucsb.edu  
tsoh@engr.ucsb.edu

Dr. A. Csordas<sup>[†]</sup>  
Institute for Collaborative Biotechnologies  
University of California, Santa Barbara (USA)


Dr. A. E. Gerdon<sup>[†]</sup>  
Department of Chemistry, Emmanuel College, Boston (USA)

J. D. Adams  
Department of Physics  
University of California, Santa Barbara (USA)

Dr. J. Qian  
Cynvenio Biosystems, Westlake Village (USA)

[†] These authors contributed equally to this work.

[\*\*] We are grateful for the financial support from the ARO Institute for Collaborative Biotechnologies, Office of Naval Research, and National Institutes of Health. We thank Xinhui Lou and Jerry Thomas for their invaluable assistance. We also thank Yanting Zhang, Paul Pagano, Marek Turewicz, and André Defusco at Cynvenio Biosystems (Westlake Village) for helpful discussions. Microfabrication was carried out in the Nanofabrication Facility at UCSB.

 Supporting information for this article (materials, aptamer design and characterization, antibody and magnetic bead preparation, MMS device fabrication and characterization, PDGF detection and real-time PCR analysis) is available on the WWW under <http://dx.doi.org/10.1002/anie.200904846>.

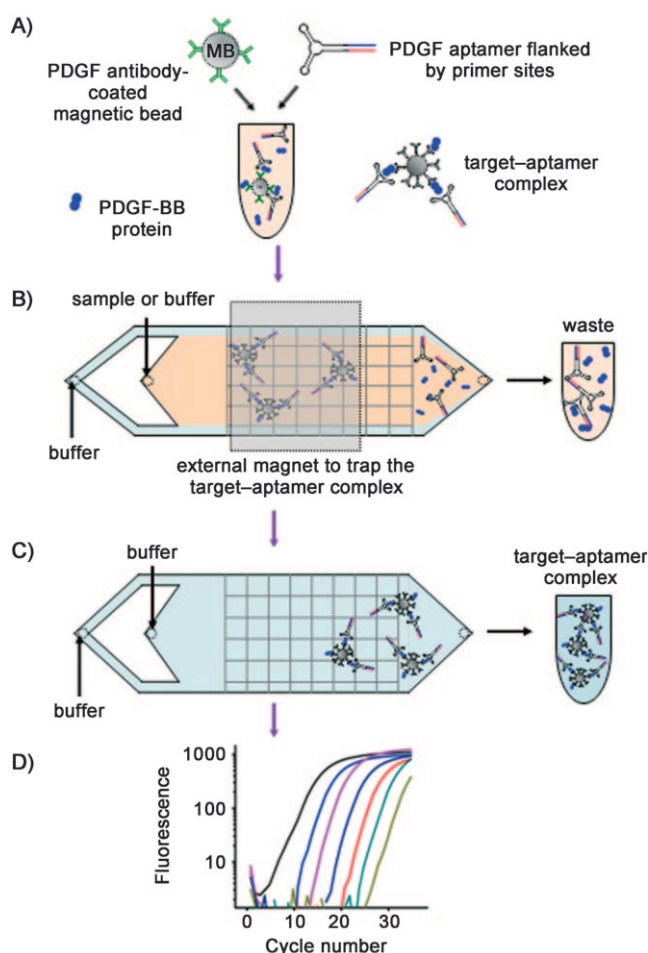


**Figure 1.** MAP assay protocol. A) Biotinylated anti-PDGF antibodies (green “Y” symbol) are immobilized on the surfaces of magnetic beads (MB). The target protein (PDGF-BB) is shown as two blue circles. The protein-binding site of the anti-PDGF PCR aptamer is shown in gray, and the primer sites are indicated in red and blue. The light orange background in the tube represents serum. B) The bead-bound target complexes are captured by the high magnetic field gradients within the MMS device, while unbound aptamers and serum proteins are continuously eluted. The light blue streams in the device represent washing buffer. C) Target complexes are eluted from the device by removal of the external magnetic field. The light blue background indicates elution buffer. D) Real-time PCR is performed on eluted samples.

interfere with the PCR amplification efficiency (see the Supporting Information, Figure S1).

To generate sufficient magnetophoretic force ( $\vec{F}_m$ ) to efficiently trap target complexes without loss and allow stringent washing, large magnetic field gradients ( $\nabla B$ ) are necessary.<sup>[21]</sup> To generate such a gradient in a controlled and reproducible manner, we created patterned ferromagnetic structures within the microchannel consisting of nickel films 200 nm in thickness<sup>[22]</sup> (Figure 2A and B). As we have previously described,<sup>[23–25]</sup> the application of an external magnetic field to the MMS device automatically generates a large localized  $\nabla B$  with magnitude of approximately  $10^5 \text{ T m}^{-1}$  within  $1 \mu\text{m}$  of the nickel grid lines, because of the significantly higher magnetic permeability of nickel relative to serum ( $\mu_{r,\text{nickel}} = 200$ ,  $\mu_{r,\text{serum}} \approx 1$ ; see the Supporting Infor-

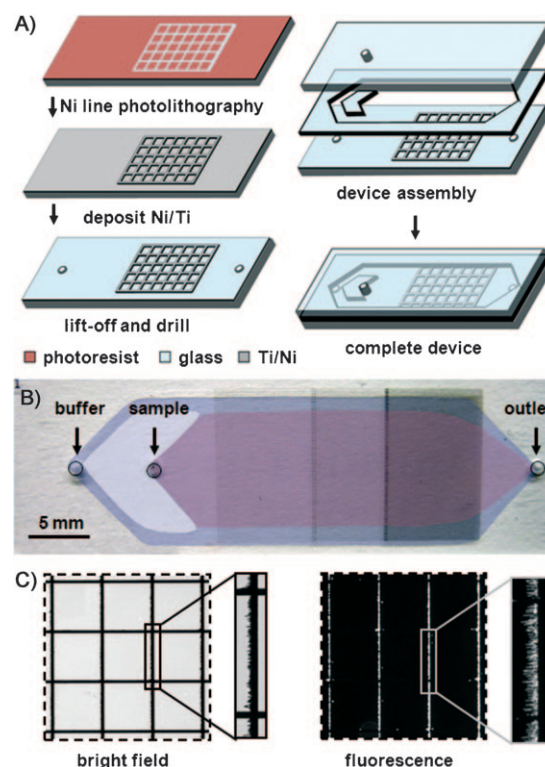


**Figure 2.** MMS device architecture and characterization. A) A multi-layer process allows reproducible fabrication of microchannels and embedded ferromagnetic structures.<sup>[25]</sup> B) Photograph of the device displaying the channel design, embedded MFSs, and fluidic path. The device dimensions are  $64 \times 15.7 \times 1.5 \text{ mm}^3$  ( $L \times W \times H$ ) and the microfluidic channel has a height of  $30 \mu\text{m}$  and a width of  $12 \text{ mm}$ . C) Bright-field and fluorescence micrographs demonstrate that the magnetic beads are trapped at the edges of the MFS patterns where the magnetic field gradients are the largest.

mation, Figure S2). Assuming a saturation magnetization ( $m$ ) of  $2.3 \times 10^{-14} \text{ A m}^2$  for the magnetic beads, we estimate the lower bound of the magnetophoretic trapping force on the magnetic target complexes ( $\vec{F}_m = m \nabla B$ ) to be about 2 nN. On the other hand, the fluidic drag force ( $\vec{F}_d$ ) on a spherical magnetic bead can be approximated by the Stokes drag equation  $\vec{F}_d = 6\pi\eta r \vec{v}_f$ , where  $\eta$  is the fluid viscosity,  $r$  is the radius of the bead, and  $\vec{v}_f$  is the velocity of the fluid. Under typical MMS operation conditions, the maximum volumetric throughput is about  $14 \text{ mL h}^{-1}$  (during the washing step), which would exert an upper bound of  $\vec{F}_d \approx 0.14 \text{ nN}$ , thus confirming that the condition  $\vec{F}_m > \vec{F}_d$  is satisfied. This capability provides a reproducible mechanism to stringently wash away the PCR inhibitors and unbound aptamer reagents in the sample, while retaining the target complexes virtually without loss (Figure 2C). Notably, most of the magnetic target complexes were trapped at the edges of the MFS patterns, where the magnetic field gradient is the strongest.<sup>[21]</sup>

To determine the sensitivity of the assay, we performed calibration experiments in triplicate with PDGF-BB in both PBSM and fetal bovine serum (FBS) over a target concentration range of 10 fM to 1 nM (Figure 3). Following amplification, a dissociation analysis was performed to verify that only expected target sequences were amplified (see the

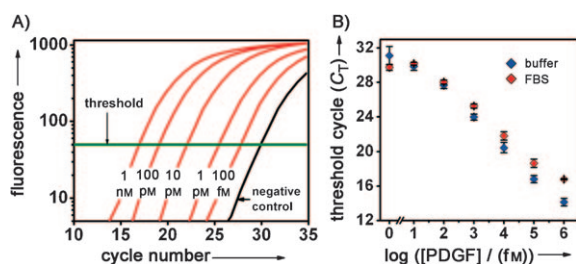


**Figure 3.** MAP assay sensitivity. A) Amplification results from different PDGF-BB concentrations in 20% FBS. The 100 fM PDGF-BB amplification plot is clearly distinguishable from that for the negative control. B) Threshold cycle values are plotted as a function of the log<sub>10</sub> PDGF-BB concentration in fM. Negative (no protein) control values are shown to the left of the 10 fM concentrations.

Supporting Information, Figure S3), an essential step when using nonspecific double-stranded DNA (dsDNA) binding dyes such as SYBR Green in real-time PCR. This process is rapid and facile, as amplification and specificity analysis were completed in less than one hour. As expected, the threshold cycle values decreased monotonically with increasing protein concentration, which indicates that the target protein concentration is directly proportional to the aptamer copy number. The results were reproducible and the magnitudes of the signals were large, spanning nearly 14 cycles (equivalent to an approximately 10000-fold change in the aptamer copy number) from 10 fM to 1 nM of target concentration.

The MAP assay shows a sigmoidal response as a function of target concentration (Figure 3B), as expected from sandwich assays such as ELISA<sup>[26]</sup> and immuno-PCR.<sup>[27]</sup> To determine the limit of detection, we first obtained the standard deviation of the signals from the negative control samples. Next, we fitted the calibration data in Figure 3B with a third-order polynomial<sup>[28]</sup> and obtained a high correlation coefficient of regression within our operating range ( $R^2 > 0.99$ ). Finally, the standard deviation value was multiplied by 3<sup>[29]</sup> and subtracted from the mean negative control reaction signal to arrive at limits of detection (LODs) of 72 and 62 fM in buffer and 20% serum, respectively.

The specificity of the MAP assay was evaluated by analysis of 100 pM PDGF-BB, PDGF-AB, or PDGF-AA in PBSM buffer containing 0.37% bovine serum albumin (BSA). We also tested human serum albumin (HSA) at a concentration of 0.005% (750 nM) in PBSM buffer with 0.37% BSA. Experiments were also conducted without magnetic beads or using magnetic beads with a polyethylene glycol (PEG) coating but no capture antibody. We used  $\Delta C_T$  to quantify the signals as it directly relates to the relative difference in the nucleic acid template copy number between two samples,<sup>[30,31]</sup> with  $\Delta C_T$  defined here as the difference in threshold cycle value between a particular sample and the negative control. The negative control reactions contain antibody-coated beads and anti-PDGF PCR aptamers without the target protein.

The MAP assay demonstrates remarkable specificity (Figure 4); for example,  $\Delta C_T$  between the negative control and the HSA sample was 0.1, which indicates that HSA does not yield a false-positive signal in our system. In addition, a

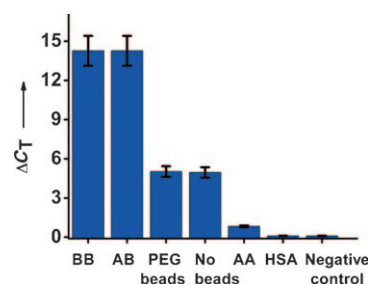


**Figure 4.** Assay specificity as measured by the change in PCR threshold cycles. The samples tested were: 100 pM PDGF-BB, 100 pM PDGF-AB, PEG-coated beads with 100 pM PDGF-BB, 100 pM PDGF-BB with no beads, 100 pM PDGF-AA, 0.005% HSA, and a negative control containing no protein.

$\Delta C_T$  value of less than 1 was observed between the negative control and a PDGF-AA sample, thus indicating that our system is specific to PDGF-BB and does not bind PDGF-AA, in agreement with literature reports of negligible binding to PDGF-AA.<sup>[32–34]</sup> The signals from the samples containing PDGF-BB and PDGF-AB proteins were remarkably similar in magnitude ( $\Delta C_T = 14.27$ ); this result is consistent with the facts that the dissociation constants ( $K_d$ ) of the aptamer are nearly identical for both isoforms,<sup>[31,35]</sup> and the capture antibody can be used for the detection of either isoform. We measured  $\Delta C_T$  values of 5.03 and 4.96 for PEG-coated beads and the sample without beads, respectively. Though significant, the two signals are approximately 500-fold smaller than the signal from a test sample containing 100 pM of PDGF-BB target, based on aptamer copy number. We believe these small signals originate from proteins and aptamers that are nonspecifically bound to the beads and the chamber of the MMS device during the separation step.

We have demonstrated the capability to quantitatively detect low-femtomolar concentrations of target proteins directly in serum samples using a microfluidic sample preparation system with DNA aptamers containing PCR primer sequences. The chip-based, high-gradient magnetic separation system facilitated efficient elimination of unused reagents and PCR inhibitors from the serum sample, thus enabling quantitative real-time PCR readout. By using an aptamer as an affinity and amplification reagent, the complex conjugation steps required in related methods such as immuno-PCR were avoided. Based on experiments, we believe that aptamers with  $K_d$  values in the low-nanomolar range are sufficient for our method to work reliably. For example, the PDGF aptamer used has a  $K_d$  of approximately 0.1 nM as reported by Green et al.<sup>[35]</sup>

Aptamers are well suited for real-time PCR because of their small size (<100 nucleotides), which results in high-efficiency amplification, and the capacity to modify their 3' and 5' ends with user-defined sequences allows for the design of highly target-specific primers, ultimately leading to a significant increase in assay sensitivity and multiplexing capability. As with most dual-recognition approaches, we suspect that the aptamer and antibody must have non-overlapping binding sites for the method to work effectively. We obtained a LOD of 62 fM for PDGF-BB in FBS, with a



large dynamic range that spanned approximately five orders of magnitude (62 fm to 1 nm). The sensitivity of our assay compares favorably with previous efforts using the same PDGF-BB-binding aptamer; for example, a light-switching excimer probe offered a detection limit of 2.5 nM in 10 % cell media,<sup>[36]</sup> while an electrochemical approach yielded a detection limit of 50 pM in 50 % serum.<sup>[32]</sup> By using a detection scheme that incorporates real-time PCR, Yang and Ellington detected PDGF-BB with a LOD of 12.8 pM in the presence of 1 µg mL<sup>-1</sup> fibroblast cell lysate,<sup>[31]</sup> and low-femtomolar detection limits were obtained with a proximity ligation assay<sup>[34]</sup> and a rolling-circle amplification-based method using an antibody–aptamer pair.<sup>[37]</sup>

Microfluidics technology is well suited for integrated sample preparation because it allows for precise and reproducible control of magnetic and fluidic forces in a disposable chip format.<sup>[38]</sup> In our system, we designed the device such that the magnetic force on the target complex is always larger than the fluidic drag force, thus allowing high stringency and continuous washing with minimal loss of magnetic beads. This is important because continuous washing (that is, material removal) seems to be significantly more efficient than fixed-volume washing (that is, dilution) in removing nonspecifically bound contaminants.<sup>[39]</sup> For example, our approach obtained a LOD that is approximately two orders of magnitude lower than that for a similar system that used fixed-volume washing.<sup>[40]</sup> We hypothesize that the higher washing efficiency originates from the fluidic shear forces, as well as the elimination of rebinding of contaminants, which would otherwise occur in a fixed-volume wash. In addition, the capability to reproducibly generate remarkably high magnetic field gradients ( $> 10^5 \text{ T m}^{-1}$ ) enables high volumetric throughputs (14 mL h<sup>-1</sup> per microchannel) that can be readily increased through parallel operation.

Finally, the MAP system can be readily expanded for multiplexed detection of other protein biomarkers as well as other types of targets (e.g., small molecules, viruses, and bacteria) through appropriate design of the aptamers. We believe such advancements will represent a significant step toward care diagnostics and personalized medicine at the point of care.

Received: August 30, 2009

Published online: December 3, 2009

**Keywords:** analytical methods · aptamers · growth factors · polymerase chain reaction · proteins

- [1] L. Hartwell, D. Mankoff, A. Paulovich, S. Ramsey, E. Swisher, *Nat. Biotechnol.* **2006**, *24*, 905.
- [2] J. Yu, C. Ustach, H.-R. C. Kim, *J. Biochem. Mol. Biol.* **2003**, *36*, 49.
- [3] Y. Amano, Q. Cheng, *Anal. Bioanal. Chem.* **2005**, *381*, 156.
- [4] N. L. Anderson, N. G. Anderson, *Mol. Cell. Proteomics* **2002**, *1*, 845.
- [5] L. Thadikaran, M. A. Siegenthaler, D. Crettaz, P.-A. Queloz, P. Schneider, J.-D. Tissot, *Proteomics* **2005**, *5*, 3019.
- [6] K. N. Baker, M. H. Rendall, A. Patel, P. Boyd, M. Hoare, R. B. Freedman, D. C. James, *Trends Biotechnol.* **2002**, *20*, 149.
- [7] G. P. Manukyan, K. A. Ghazaryan, Z. A. Ktsoyan, M. V. Tatyán, Z. A. Khachatryan, G. S. Hakobyan, V. A. Mkrtchyan, D. Kelly, A. Coutts, R. I. Aminov, *Clin. Biochem.* **2008**, *41*, 920.
- [8] A. Greystoke, J. Cummings, T. Ward, K. Simpson, A. Renahan, F. Butt, D. Moore, J. Gietema, F. Blackhall, M. Ranson, A. Hughes, C. Dive, *Ann. Oncol.* **2008**, *19*, 990.
- [9] J. R. Layshock in *Analytical Techniques for Biopharmaceutical Development* (Eds.: T. Wehr, R. Rodriguez-Diaz, S. Tuck), Marcel Dekker, New York, **2005**, p. 412.
- [10] M. T. Lam, Q. H. Wan, C. A. Boulet, X. C. Le, *J. Chromatogr. A* **1999**, *853*, 545.
- [11] M. Gullberg, S. M. Gustafsdottir, E. Schallmeiner, J. Jarvius, M. Bjarnegard, C. Betsholtz, U. Landegren, S. Fredriksson, *Proc. Natl. Acad. Sci. USA* **2004**, *101*, 8420.
- [12] Y.-C. Guo, Y.-F. Zhou, X.-E. Zhang, Z.-P. Zhang, Y.-M. Qiao, L.-J. Bi, J.-K. Wen, M.-F. Liang, J.-B. Zhang, *Nucleic Acids Res.* **2006**, *34*, e62.
- [13] C. M. Niemeyer, M. Adler, R. Wacker, *Trends Biotechnol.* **2005**, *23*, 208.
- [14] T. Sano, C. L. Smith, C. R. Cantor, *Science* **1992**, *258*, 120.
- [15] J.-M. Nam, C. S. Thaxton, C. A. Mirkin, *Science* **2003**, *301*, 1884.
- [16] W. A. Al-Soud, L. J. Jönsson, P. Rådström, *J. Clin. Microbiol.* **2000**, *38*, 345.
- [17] W. A. Al-Soud, P. Rådström, *Appl. Environ. Microbiol.* **1998**, *64*, 3748.
- [18] W. A. Al-Soud, P. Rådström, *J. Clin. Microbiol.* **2001**, *39*, 485.
- [19] I. G. Wilson, *Appl. Environ. Microbiol.* **1997**, *63*, 3741.
- [20] J. R. Crowther, *The ELISA Guidebook*, Vol. 149, Humana, Totowa, NJ, **2001**.
- [21] J. D. Adams, U. Kim, H. T. Soh, *Proc. Natl. Acad. Sci. USA* **2008**, *105*, 18165.
- [22] D. W. Inglis, R. Riehn, R. H. Austin, J. C. Sturm, *Appl. Phys. Lett.* **2004**, *85*, 5093.
- [23] Y. Liu, J. D. Adams, K. Turner, F. V. Cochran, S. S. Gambhir, H. T. Soh, *Lab Chip* **2009**, *9*, 1033.
- [24] X. Lou, J. Qian, Y. Xiao, L. Viel, A. E. Gerdon, E. T. Lagally, P. Atzberger, T. M. Tarasow, A. J. Heeger, H. T. Soh, *Proc. Natl. Acad. Sci. USA* **2009**, *106*, 2989.
- [25] J. Qian, X. Lou, Y. Zhang, Y. Xiao, H. T. Soh, *Anal. Chem.* **2009**, *81*, 5490.
- [26] A. Knopp, D. Knopp, R. Niessner, *Environ. Sci. Technol.* **1999**, *33*, 358.
- [27] K. Lind, M. Kubista, *J. Immunol. Methods* **2005**, *304*, 107.
- [28] R. A. Herman, P. N. Scherer, G. Shan, *J. Immunol. Methods* **2008**, *339*, 245.
- [29] ACS Committee on Environmental Improvement, *Anal. Chem.* **1980**, *52*, 2242.
- [30] P. S. Bernard, C. T. Wittwer, *Clin. Chem.* **2002**, *48*, 1178.
- [31] L. Yang, A. D. Ellington, *Anal. Biochem.* **2008**, *380*, 164.
- [32] R. Y. Lai, K. W. Plaxco, A. J. Heeger, *Anal. Chem.* **2007**, *79*, 229.
- [33] C. Zhou, Y. Jiang, S. Hou, B. Ma, X. Fang, M. Li, *Anal. Bioanal. Chem.* **2006**, *384*, 1175.
- [34] S. Fredriksson, M. Gullberg, J. Jarvius, C. Olsson, K. Pietras, S. M. Gustafsdottir, A. Östman, U. Landegren, *Nat. Biotechnol.* **2002**, *20*, 473.
- [35] L. S. Green, D. Jellinek, R. Jenison, A. Östman, C.-H. Heldin, N. Janjic, *Biochemistry* **1996**, *35*, 14413.
- [36] C. J. Yang, S. Jockusch, M. Vicens, N. J. Turro, W. Tan, *Proc. Natl. Acad. Sci. USA* **2005**, *102*, 17278.
- [37] L. Zhou, L.-J. Ou, X. Chu, G.-L. Shen, R.-Q. Yu, *Anal. Chem.* **2007**, *79*, 7492.
- [38] J. D. Adams, H. T. Soh, *JALA* **2009**, *14*, 331.
- [39] S. P. Mulvaney, C. L. Cole, M. D. Kniller, M. Malito, C. R. Tamanaha, J. C. Rife, M. W. Stanton, L. J. Whitman, *Biosens. Bioelectron.* **2007**, *23*, 191.
- [40] N. O. Fischer, T. M. Tarasow, J. B. H. Tok, *Anal. Biochem.* **2008**, *373*, 121.